Adrian Barnes*

A Comparison of Structural Models of $Tb_3Al_5O_{12}$ and $Nd_3Al_5O_{12}$ Glasses Obtained When Using X-ray Data Alone and When X-ray and Neutron Data are Combined

DOI 10.1515/zpch-2015-0668
Received July 27, 2015; accepted September 29, 2015

Abstract: X-ray diffraction experiments, including Anomalous X-ray Diffraction, have been carried out on $Tb_3Al_5O_{12}$ and $Nd_3Al_5O_{12}$ glasses. In addition, neutron diffraction and isotopic substitution experiments have been carried out for $Nd_3Al_5O_{12}$. The data has been analysed by direct Fourier transform methods and by refinement of atomistic structures obtained from Molecular Dynamics simulations. For $Nd_3Al_5O_{12}$ good agreement between the Molecular Dynamics simulations and all the experimental data was obtained. The Molecular Dynamics configuration was refined further using Reverse Monte Carlo methods to obtain a final atomistic configuration. The $Nd_3Al_5O_{12}$ Molecular Dynamics configuration was refined using the X-ray data alone and the results show that the final configuration was in worse agreement with the data than the original Molecular Dynamics calculation. From this result it was concluded that in order to obtain a good atomistic model of $Tb_3Al_5O_{12}$ it is essential to include at least one neutron diffraction measurement in the Molecular Dynamics – Reverse Monte Carlo refinement.

Keywords: Anomalous X-ray Scattering, Neutron Scattering, Isotopic Substitution, Glass, Molecular Dynamics, RMC Refinement.

1 Introduction

The physical and optical properties of glasses are closely related to the atomic structure of the glass including the network topology, the effect of network modifiers and the inclusion of ions into network structure. Hence the direct determination of the structural motifs and their connectivity, the coordination of modifier ions in the network and the position of other charged ions in the network are all important pieces of structural information needed to improve our understanding of their behaviour [1, 2]. However, in an n-components system, even simple information such as coordination numbers and bond lengths are difficult to obtain from a single diffraction pattern of a glass due to the overlapping contributions of the $N = n(n+1)/2$ atom-atom pair correlations in the diffraction patterns and their associated reciprocal space partial structure factors [3]. The situation may be improved by noting in the case of both X-ray and neutron diffraction that the relative contribution of each $S_{\alpha\beta}(Q)$ to the measured diffraction pattern can be altered by changing, for example, the wavelength of the radiation used, or, in the case of neutrons, the isotopic composition of the elements in the sample. The technique of neutron diffraction and isotopic substitution (NDIS) has been used extensively to obtain atom specific information in many disordered materials. In contrast the X-ray equivalent, Anomalous X-ray Diffraction (AXD) has been used in only a limited number of cases, largely due to the technical difficulties in doing accurate measurements.

NDIS has been successfully applied to a large number of binary ($n = 2$) liquids and glasses where individual partial structure factors may be determined unambiguously by measurement of $N = 3$ samples of different isotopic compositions [3]. The formal solution of the problem then involves the inversion of a 3×3 matrix. The method has also been extended to experiments in which X-ray diffraction and NDIS [4], AXD and a single neutron diffraction measurement [5], and multiwavelength AXD measurements have been combined [6].

However, when the number of component elements in the material exceeds two, the direct determination of the partial structure factors is no longer feasible due to the poor conditioning of the inverse matrix and the large numerical errors this introduces. For example, in the case of $n = 3$ there are $N = 6$ partial structure factors that need to be obtained by 6 independent measurements and the inversion of a 6×6 matrix. In these systems measurements have been largely restricted to *difference* experiments in which the correlations to particular target elements are obtained. Hence, in these cases there are no realistic experimental methods that can be used to unambiguously determine *all* the partial structure factors of the system [3].

Computer simulations including, Monte Carlo (MC), Molecular Dynamics (MD) and *ab initio* Molecular Dynamics (AIMD) are increasingly used to model the structure of liquids and glasses, see for example, Reference [7]. Inherent in these methods is the ability to generate theoretical partial structures for the material. These can then be used to construct theoretical X-ray or neutron diffraction patterns that can be directly compared to experiment. The level of agreement with the experimental data is then used to validate the accuracy of the simulation.

***Corresponding author: Adrian Barnes,** H. H. Wills Physics Department, Royal Fort, Tyndall Avenue, BS8 1TL Bristol, United Kingdom, e-mail: a.c.barnes@bristol.ac.uk

Bereitgestellt von | Philipps-Universitätsbibliothek Marburg
Angemeldet
Heruntergeladen am | 24.04.16 17:32

However, perfect agreement is difficult to achieve and comparison at the level of a single diffraction experiment does not always reveal any subtle, but perhaps important, correlations in the material.

In recent years the bridge between experiment and simulation has been addressed by structural refinement methods based on the Reverse Monte-Carlo (RMC) method whereby the theoretical structural model is refined by making random small changes in the atom configuration to obtain closer agreement with the experimental data [8]. The justification for the method is predicated on the basis that provided the displacement of the atoms from the original positions is small (less than a typical inter-atomic spacing) then the basic structure is unchanged. A direct analogy is crystal structure refinement by the Rietveld method. However, the effectiveness of the method depends on two factors: the degree of the initial agreement between the simulation and experimental data and the information content in the experimental data.

In this paper we explore the issue of information content with regard to measurements of the structure of two related rare earth aluminate glasses, namely $Tb_3Al_5O_{12}$ and $Nd_3Al_5O_{12}$. In particular we address how the addition of explicit atom specific information such as AXD and NDIS improves the reliability of the refined models and we also explore issues that should guide the planning of future experiments.

2 Theory

2.1 Diffraction

The diffraction pattern obtained from a glass, after correction for experimental effects (self-absorption, multiple scattering ...) may be written as,

$$F^T(Q) = \sum_{\alpha}\sum_{\beta} c_\alpha c_\beta w^*_\alpha(Q) w_\beta(Q)[S_{\alpha\beta}(Q) - 1], \tag{1}$$

where c_α, c_β are the atomic concentrations of species α and β respectively, $w_\alpha(Q), w_\beta(Q)$ are the atomic scattering factors, $S_{\alpha\beta}(Q)$ are the partial Faber-Ziman structure factors corresponding to the correlations between species α and β [3] and the superscript T means 'Total Structure Factor'. In a neutron scattering experiment $w_\alpha(Q)$, $w_\beta(Q)$ are the neutron coherent scattering lengths b_α and b_β that are independent of Q and the incident neutron energy (apart from a small number of cases (e.g. Cd) where a strong nuclear resonance near thermal neutron energies occurs). In an X-ray scattering experiment w_α and w_β are the X-ray form factors f_α and f_β for the atoms. The X-ray form factor may be further separated

into a term $f_0(Q)$ that is related to the average electron density in the atom (or ion) and the dispersion terms f' and f'' that vary strongly around the X-ray absorption edge of the atom. Hence $w(Q)$ may be written in complex number form as,

$$w(Q) = f_0(Q) + f' + if''. \tag{2}$$

It can be seen from Equation (1) that the measured diffraction pattern, for a given composition, will change when $w(Q)$ is changed by, for example, changing the isotope (neutrons) or the wavelength around an absorption edge (X-rays or neutrons). Hence in principle, it is possible to determine the individual partial structure factors, by making $n(n+1)/2$ independent diffraction measurements to determine the $n(n+1)/2$ unknown $S_{\alpha\beta}(Q)$. In practise, apart from some binary compounds, the direct inversion of diffraction data to obtain partial structures in this way is not possible due to the limited statistical accuracy of the data and the ill conditioning of the inverse matrix.

In the case that only one $w_\alpha(Q)$ is varied (i.e. a single isotopic substitution or a measurement at two wavelengths for the case of AXD), a First Order Difference (FOD) function that gives the specific atom correlations around the substituted atom may be determined by a simple subtraction of the two diffraction patterns,

$$\begin{aligned} F^{FOD}_\alpha(Q) = F_1(Q) - F_2(Q) = \\ c^2_\alpha\left([w_{\alpha1}]^2 - \left[w^2_{\alpha2}\right]\right)(S_{\alpha\alpha}(Q) - 1) + \\ \sum_{\beta,\beta\neq\alpha} c_\alpha c_\beta\left(\left[w^*_{\alpha1}w_\beta + w^*_\beta w_{\alpha1}\right] - \left[w^*_{\alpha2}w_\beta + w^*_\beta w_{\alpha2}\right]\right) \\ \times (S_{\alpha\beta}(Q) - 1), \end{aligned} \tag{3}$$

where $w_{\alpha1}$ and $w_{\alpha2}$ represent the change in the scattering factor from the isotopic substitution or wavelength change. The explicit Q dependence of w has been omitted for clarity and it is assumed that the $w_{\beta,\beta\neq\alpha}$ do not change. A second difference, the Total Minus Weighted Difference ($TMWD$) function,

$$\begin{aligned} F^{TMWD}_\alpha(Q) = ((w_{\alpha2}w^*_\beta + w^*_{\alpha2}w_\beta)F_1(Q) - \\ (w_{\alpha1}w^*_\beta + w^*_{\alpha1}w_\beta)F_2(Q)), \end{aligned} \tag{4}$$

where $\beta \neq \alpha$ may also be defined. Careful algebra in this case shows that the weighting of all the $S_{\alpha\beta}(Q)(\alpha \neq \beta)$ where α is the substituted atom, are zero such that this function is broadly complementary to $F^{FOD}(Q)$. It may however be noted that $F^{FOD}(Q)$ and $F^{TMWD}(Q)$ both contain a contribution from $S_{\alpha\alpha}(Q)$.

$F^T(Q)$, $F^{FOD}(Q)$ and $F^{TMWD}(Q)$ may be transformed to real-space by the Fourier transform,

$$G^X(r) = \frac{1}{2\pi^2\rho r}\int_0^\infty F^X(Q)\cdot Q\cdot \sin(Qr)\mathrm{d}Q, \tag{5}$$

where $X = (T, FOD \text{ or } TMWD)$ and $G^X(r)$ consists of the weighted average of the partial radial distribution functions $g_{\alpha\beta}(r)$ that are related to the partial structure factors by the transform,

$$g_{\alpha\beta}(r) = \frac{1}{2\pi^2\rho r}\int_0^\infty Q\cdot(S_{\alpha\beta}(Q)-1)\sin(Qr)\mathrm{d}Q \tag{6}$$

The Q dependent $w_{\alpha\beta}(Q)$ for the X-ray case act as a modifying function $M(Q)$ on $S_{\alpha\beta}(Q) - 1$ in Equation (6). The Fourier transform in in Equation (6) results in broadened peaks in real space [9]. It is common to normalise $F^X(Q)$ according to the Faber–Ziman scheme,

$$S^X(Q) - 1 = \frac{F^X(Q)}{|W(Q)|^2} \tag{7}$$

where $W(Q)$ is the sum of the Q dependent weighting terms in the corresponding $F^X(Q)$. This representation has advantages and disadvantages for the case of X-ray diffraction. Direct Fourier transformation of Equation (5) gives broad peaks in real space due to the effect of the Q-dependence of the X-ray form factors. Hence it is difficult to resolve closely spaced peaks in real space. The normalisation used in Equation (7) has the effect of lessening this Q-dependence by dividing by an average Q-dependent form factor. In this way the real space resolution may be improved, but it must be recognised that this procedure does not result in a completely Q-independent weighting of each partial structure term and may lead to unwanted artifacts in the Fourier transform. Furthermore, in extreme cases, for example $S^{TMWD}(Q)$, this normalization scheme still results in a heavy Q dependence of the weighting factors (see for example Figure 1). In this paper we always present these normalised total structure factors ($S^T(Q)$, $^{FOD}(Q)$ and $S^{TMWD}(Q)$) and their related $G^T(r)$, $G^{FOD}(r)$ and $G^{TMWD}(r)$. It is this problem of the Q dependence of the X-ray form factors that limits the ability to determine accurate bond distances and coordination numbers by Fourier Transform in the case of X-ray diffraction.

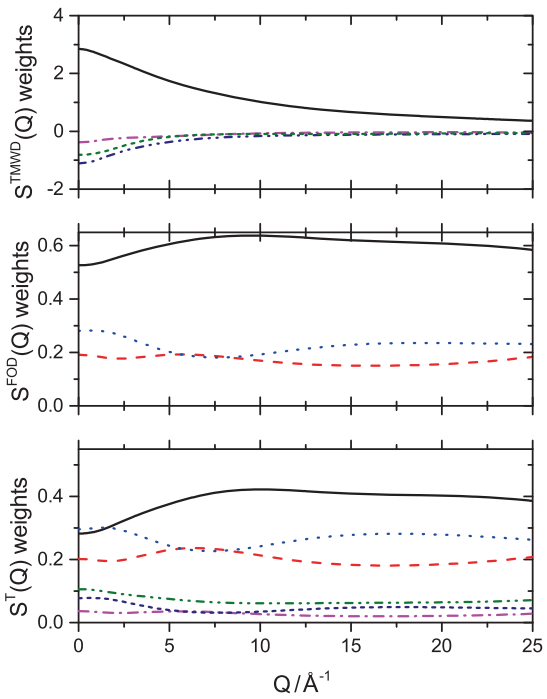

Figure 1: The X-ray weightings for the partial structure factors in $F^T(Q)$, $F^{FOD}(Q)$ and $F^{TMWD}(Q)$ for $Tb_3Al_5O_{12}$ glass. The correlations are: Tb-Tb – solid (black), Tb-Al – dashed (red), Tb-O – dotted (blue), Al-Al – dot-dash (magenta), Al-O – dot-dot-dash (dark green) and O-O – short dash (dark blue) lines respectively. The relative weights for $Nd_3Al_5O_{12}$ glass are similar and not reproduced here.

2.2 Modelling

An alternative approach to analysing diffraction data by direct Fourier transform methods is to take theoretical calculations, primarily Monte Carlo or Molecular Dynamics simulations, to compare the experimentally measured data with that predicted directly from these models. A good agreement between the experiment and simulation is then used to justify an interpretation of the structure based on the simulation configurations.

In practise there is never a perfect agreement between experiment and theoretical models and what constitutes *good agreement* is open to interpretation.

Hence, it has become common practise to use the simulation configuration as the starting point for a refinement of the structure by, for example, Reverse Monte Carlo (RMC) methods. With Molecular Dynamics and RMC procedures (MD-RMC) excellent agreement between the experimental data and the model configuration is often achieved [8, 10].

The robustness of these refinement procedures depends strongly on the amount of experimental data included. Refinement of a single X-ray or neutron diffraction experiment puts relatively little constraint on the atomic configuration such that although good fits to the data are obtained, structural details may be missed. Hence, in practice, the more element specific information included in the refinement the more reliable the resulting model structures will be.

This modelling/fitting approach has significant advantages when X-ray data is included as the refinement procedure does not involve any ambiguities in interpretation due to the problem of dealing with Q-dependent X-ray form factors as noted in Section 2.1. The method therefore lends itself to combining a single neutron experiment with a single X-ray experiment where direct difference functions may not be obtained. Furthermore, it leads naturally and easily to adding further constraints from additional NDIS and/or AXD measurements as well as spectroscopic data from, for example, EXAFS or NMR.

3 Methods

3.1 Diffraction experiments

Samples of $Tb_3Al_5O_{12}$ and $Nd_3Al_5O_{12}$ glass were fabricated from pure Tb_2O_3 or Nd_2O_3 and Al_2O_3 powders. The initial material was formed on a copper hearth by laser heating. The glasses were then formed using the method of aerodynamic levitation and laser heating by direct quenching from the melt at 2500 K which gives a cooling rate of $\sim 300\ \mathrm{K \cdot s^{-1}}$. Details of the preparation of glasses by this method have been given in reference [8]. In addition a further sample of $Nd_3Al_5O_{12}$ was fabricated using ^{146}Nd isotope (97.6% enrichment) by this method.

X-ray diffraction experiments were carried out using beamline ID31 at the ESRF (European Synchrotron Radiation Facility, Grenoble, France) at energies of 51 596 eV and 51 956 eV (400 and 40 eV below the Tb K absorption edge respectively) and 43 196 eV and 43 556 eV (400 and 40 eV below the Nd K absorption edge respectively). The incident energy resolution was approximately 1 eV. The instrument 9 channel Si(111) monochromator was used to obtain a scattered beam energy resolution of a few hundred eV in order to eliminate an issues arising from

Table 1: The potential parameters used in the MD simulation.

Buckingham Potentials used for $Tb_3Al_5O_{12}$			
Pair	$A_{\alpha\beta}$ (eV)	$B_{\alpha\beta}$ ($\mathrm{Å^{-1}}$)	$C_{\alpha\beta}$ ($\mathrm{eV\,Å^{-6}}$)
Tb^{3}-O^{-2}	845.137	0.3750	0.00
Al^{3}-O^{-2}	2409.505	0.2649	0.00
O^{-2}-O^{-2}	25.410	0.6937	32.32

Morse potentials used for $Nd_3Al_5O_{12}$				
Pair	$D_{\alpha\beta}$ (eV)	$a_{\alpha\beta}$ ($\mathrm{Å^{-2}}$)	r_o (Å)	$C_{\alpha\beta}$ ($\mathrm{eV\,Å^{-12}}$)
$Nd^{1.8}$-$O^{-1.2}$	0.014580	1.825100	3.398717	3.0
$Al^{1.8}$-$O^{-1.2}$	0.361581	1.900442	2.164818	0.9
$O^{-1.2}$-$O^{-1.2}$	0.042395	1.379316	3.618701	22.0

resonance raman emission close to the absorption edges and to reduce Compton scattering at high scattering angles.

Neutron diffraction experiments were carried out at the ILL (Institut Laue-Langevin, Grenoble, France) using the D4C diffractometer with an incident wavelength of 0.4998 Å. The measurements were made using approximately 50 glass beads of equal mass produced under identical conditions. The beads were placed in a cylindrical vanadium cylinder (0.1 mm thickness). Standard attenuation, multiple scattering and placzek corrections were made and the data normalized with respect to a standard vanadium sample [11]. After normalization the data was corrected for the paramagnetic scattering contribution arising from moment of the Nd ion [12]. The neutron scattering lengths used in the data analysis were $b_{\mathrm{O}} = 5.803$ fm, $b_{\mathrm{Al}} = 3.449$ fm, $b_{\mathrm{Nd}^{nat}} = 7.69$ fm and $b_{\mathrm{Nd}^{146}} = 8.45$ fm.

3.2 Simulation and modelling methods

Molecular dynamics simulations of $Tb_3Al_5O_{12}$ and $Nd_3Al_5O_{12}$ were carried out using DL_POLY [13, 14]. Buckingham potentials [15]

$$\phi_{\alpha\beta}(r_{\alpha\beta}) = A_{\alpha\beta}\exp\left(-\frac{r_{\alpha\beta}}{\rho_{\alpha\beta}}\right) - \frac{C_{\alpha\beta}}{r_{\alpha\beta}^6} + \frac{q_\alpha q_\beta}{4\pi\epsilon_0 r}, \tag{8}$$

and Morse potentials [16]

$$\phi_{\alpha\beta}(r_{\alpha\beta}) = D_{\alpha\beta}\left[\left\{1-\exp\left(-\left(\frac{a_{\alpha\beta}}{r_{\alpha\beta}-r_0}\right)\right)\right\}^2 - 1\right] + \frac{C_{\alpha\beta}}{r_{\alpha\beta}^{12}} \tag{9}$$

have been used. Previous studies [17] have suggested that the Morse potentials give a better initial agreement with the data than the Buckingham potentials. However, suitable Morse potentials for Tb-O could not be found in the literature so we have used the Morse potentials of Pedone et al. [16] for the $Nd_3Al_5O_{12}$ analysis and the Buckingham potentials of Bush et al. [15] for the $Tb_3Al_5O_{12}$ analysis presented here. The consequences of the use of these different potentials will be discussed later.

The parameters used in the simulations are shown in Table 1. The simulations were carried out using 5000 atoms in a cubic box of side 39.04 Å ($Tb_3Al_5O_{12}$) and 40.16 Å ($Nd_3Al_5O_{12}$) which correspond to atomic number densities of 0.084 $Å^{-3}$ and 0.077 $Å^{-3}$ respectively. Each was started from a random configuration of atoms subject to nearest neighbour distance constraints and run in the NVT ensemble using a Berensden thermostat and a timestep of 0.001 ps. The system was allowed to equilibrate for 0.5 ps and then run for a total of 50 ps. Initial runs were made at $T = 3000$ K after which the configuration was quenched to 300 K and run for a further 50 ps.

Theoretical partial $g_{\alpha\beta}(r)$ were generated from the particle positions in the final MD configuration and the partial $S_{\alpha\beta}(Q)$ were obtained by Fourier transform of Equation (6). Theoretical diffraction patterns were the obtained by summing the weighted $S_{\alpha\beta}(Q)$ using neutron scattering lengths obtained from [19] and the tabulated neutral atom form factors from the International Tables for Crystallography [20].

Structural refinement of the final MD configurations was carried out using the RMCPROFILE (version 6) programme [21]. In each case the maximum particle move allowed was 0.01 Å and nearest neighbour cut-off distances corresponding to the minimum distances found in the MD simulation were used. The refinement was run until χ^2 had reached a constant value which corresponded to about 24 h on a PC (Intel i3/2.8 Ghz processor).

4 Results

Figure 1 shows the X-ray weightings of the partial structure factors $S^T(Q)$, $S^{FOD}(Q)$ and $S^{TMWD}(Q)$ for $Tb_3Al_5O_{12}$ glass. The weightings for $Nd_3Al_5O_{12}$ are broadly similar given the closeness in atomic number of Nd and Tb and are not shown here. It is noticeable that the weighting of $S_{TbTb}(Q)$ is the strongest in all these functions. The variation in the Q-dependent form factors is apparent in the fluctuation of these weights over the Q range used in the experiments. These fluctuations mean the peak positions and shapes of the peaks in $g_{\alpha\beta}(r)$ become distorted

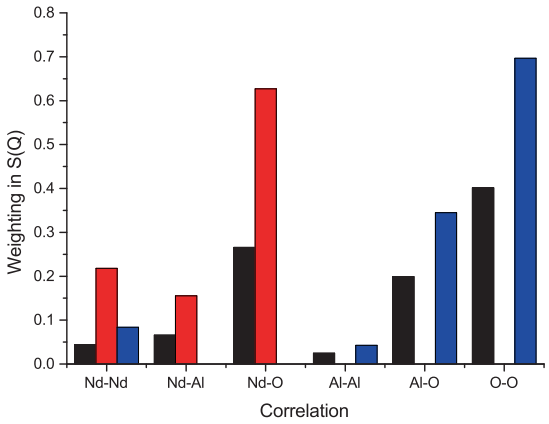

Figure 2: The neutron weightings for the partial structure factors in $S^T(Q)$, $S^{FOD}(Q)$ and $S^{TMWD}(Q)$ for $Nd_3Al_5O_{12}$ glass. $S^{FOD}(Q)$ and $S^{TMWD}(Q)$ have been calculated for ^{146}Nd isotopic substitution. Black – $S^T(Q)$, red (light grey) – $S^{FOD}(Q)$ and blue $S^{TMWD}(Q)$.

such that accurate calculations of peak positions and coordination numbers cannot be obtained reliably by direct Fourier Transform methods. In particular the rapid fall off in these weights for $S^{TMWD}(Q)$ results in highly broadened peaks in real space. It can also be noted that the strength of the Al-Al, Al-O and O-O correlations remains weak in all these functions such that information about the network Al-O structure is weak in the corresponding real space functions. Nevertheless careful integration of the first peak in $g^T(r)$ gives an Al-O coordination number of 4.0(2) for both $Tb_3Al_5O_{12}$ and $Nd_3Al_5O_{12}$. Hence, in X-ray diffraction experiments, details of the network Al-O structure are difficult to identify, even when AXD measurements are included.

Neutron scattering lengths for Nd (natural and 146), Al and O were taken from Rauch et al. [19]. Figure 2 shows the partial structure factor weightings for neutron scattering experiments. In contrast to the X-ray case it can be seen that the weighting of $S_{NdNd}(Q)$ is weak in all the structure functions (at most 20% in the First Order Difference). However, the Al-Al, Al-O and O-O network contributions are considerably larger and contribute 60% in $S^T(Q)$ and over 90% in $S^{TMWD}(Q)$. Hence the X-ray and neutron diffraction measurements give complementary information: X-rays give most on the metal coordination structure, while neutrons give more on the basic network structure.

Figure 3 shows the X-ray diffraction patterns, $S^T(Q)$, $S^{FOD}(Q)$ and $S^{TMWD}(Q)$ measured for $Tb_3Al_5O_{12}$ and $Nd_3Al_5O_{12}$. The experimental noise may be noted

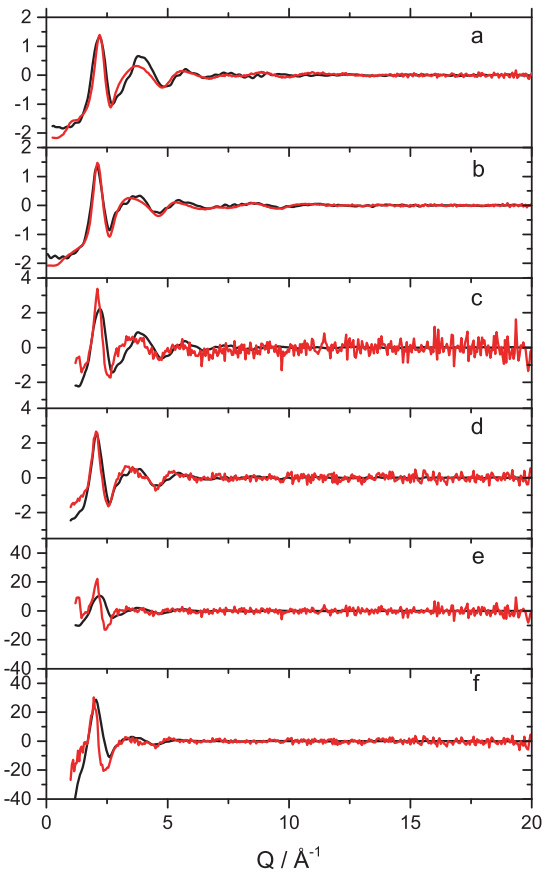

Figure 3: Comparison of the measured X-ray data (black) and the corresponding functions calculated from the MD data (red). a) $S^T(Q)$ $Tb_3Al_5O_{12}$, b) $S^T(Q)$ $Nd_3Al_5O_{12}$, c) $S^{FOD}(Q)$ $Tb_3Al_5O_{12}$, d) $S^{FOD}(Q)$ $Nd_3Al_5O_{12}$, e) $S^{TMWD}(Q)$ $Tb_3Al_5O_{12}$ and f) $S^{TMWD}(Q)$ $Nd_3Al_5O_{12}$.

particularly on the difference functions at high Q. Also shown in this figure are the corresponding theoretically predicted structure factors obtained from the MD simulation runs. The difference in agreement with the data and the MD simulations for $Tb_3Al_5O_{12}$ and $Nd_3Al_5O_{12}$ may be clearly noted and support the observation previously that the Morse potentials of Pedone et al. [16] are better for these aluminate glass systems [17].

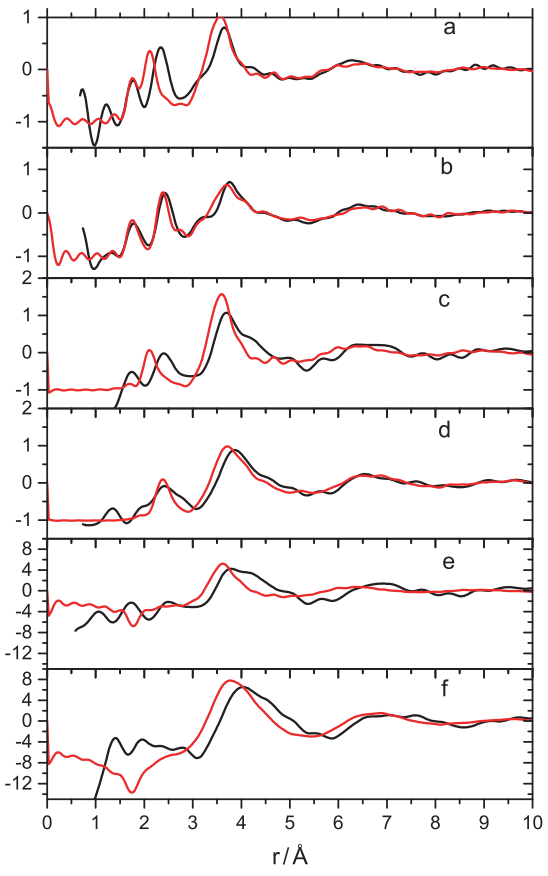

Figure 4: Comparison of the measured X-ray data (black) and the corresponding functions calculated from the MD data (red). a) $g^T(r)$ $Tb_3Al_5O_{12}$, b) $g^T(r)$ $Nd_3Al_5O_{12}$, c) $g^{FOD}(r)$ $Tb_3Al_5O_{12}$, d) $g^{FOD}(r)$ $Nd_3Al_5O_{12}$, e) $g^{TMWD}(r)$ $Tb_3Al_5O_{12}$ and f) $g^{TMWD}(r)$ $Nd_3Al_5O_{12}$.

Figure 4 shows $g^T(r)$, $g^{FOD}(r)$ and $g^{TMWD}(r)$ obtained from the Q space data shown in Figure 3. In $g^T(r)$ a clear peak corresponding to the nearest neighbour Al-O peak is observed at ~ 1.8 Å. This is followed by a peak at 2.34 Å ($Tb_3Al_5O_{12}$) and 2.42 Å ($Nd_3Al_5O_{12}$) that correspond to the nearest neighbour Tb-O and Nd-O distances respectively. The peak at ≃ 3.6 Å may be associated with the dominant correlation arising from $g_{TbTb}(r)$ and $g_{NdNd}(r)$ respectively. It can be noted

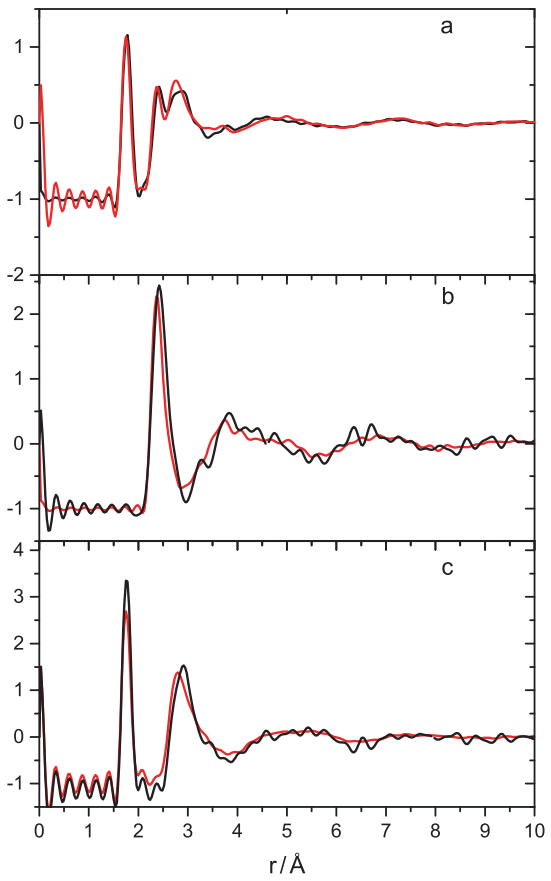

Figure 5: Comparison of the measured neutron data (black) and the corresponding functions calculated from the MD data (red) for $Nd_3Al_5O_{12}$. a) $S^T(Q)$, b) $S^{FOD}(Q)$ and c) $S^{TMWD}(Q)$.

that the short distance peaks associated with $g_{\mathrm{AlO}}(r)$ and $g_{\mathrm{NdO/TbO}}(r)$ in $g^T(r)$ are poorly resolved in the difference functions largely due to the noise on the difference data and the smoothing needed to obtain $g(r)$'s without large termination ripples and artifacts. For $Tb_3Al_5O_{12}$ the second peak in $g^T(r)$, corresponding to $g_{\mathrm{TbO}}(r)$, is displaced to a considerably shorter distance in the MD simulation than in the data – so much so that it shows some overlap with the $g_{\mathrm{AlO}}(r)$ peak. In contrast the MD simulation for $Nd_3Al_5O_{12}$ shows much closer agreement with the

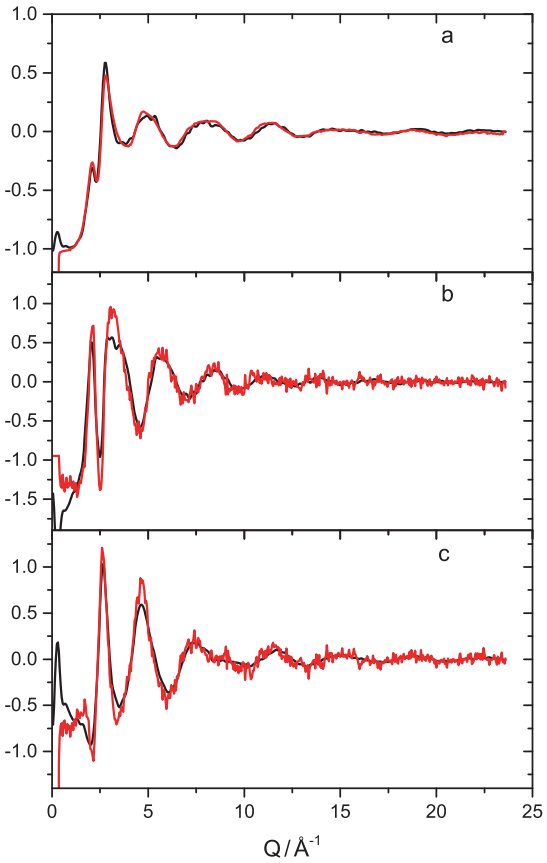

Figure 6: Comparison of the measured neutron data (black) and the corresponding functions calculated from the MD data (red) for $Nd_3Al_5O_{12}$. a) $g^T(r)$, b) $g^{FOD}(r)$ and c) $g^{TMWD}(r)$.

data. This displacement to short distance may also be observed in the $g^{FOD}(r)$ function. The implications, when interpreting the data, of the relative quality of the MD calculations will be discussed later.

Figure 5 shows the neutron diffraction pattern obtained from the natural $Nd_3Al_5O_{12}$ glass sample and $S^{FOD}(Q)$ and $S^{TMWD}(Q)$ obtained from the diffraction data including the $^{146}Nd_3Al_5O_{12}$ sample. The corresponding functions generated from the MD simulations are also shown. It may seen that there is a good

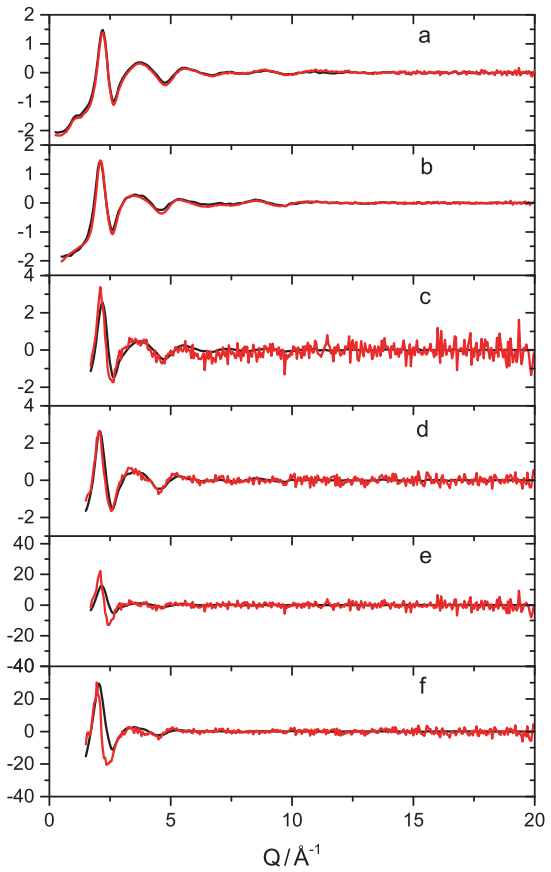

Figure 7: Comparison of the measured X-ray data (black) and the corresponding functions calculated from the MD-RMC data (red). a) $S^T(Q)$ $Tb_3Al_5O_{12}$, b) $S^T(Q)$ $Nd_3Al_5O_{12}$, c) $S^{FOD}(Q)$ $Tb_3Al_5O_{12}$, d) $S^{FOD}(Q)$ $Nd_3Al_5O_{12}$, e) $S^{TMWD}(Q)$ $Tb_3Al_5O_{12}$ and f) $S^{TMWD}(Q)$ $Nd_3Al_5O_{12}$.

level of agreement between the MD simulation and the experiment even before refining the data.

Figure 6 shows $g^T(r)$, $g^{FOD}(r)$ and $g^{TMWD}(r)$ generated from the Q-space data shown in Figure 5. $g^{FOD}(r)$ shows an isolated peak at 2.4 Å that may be associated with $g_{\mathrm{NdO}}(r)$ as there are no contributions expected from $g_{\mathrm{NdNd}}(r)$ or $g_{\mathrm{NdAl}}(r)$ at these short distances. Integration of the this peak reveals a coordination number $^{\mathrm{NdO}}_{coord} = 7.0(5)$. This peak is also observed in X-ray $g^T(r)$. In contrast to the X-ray data the peak at ≃ 3.6 Å corresponding to $g_{\mathrm{NdNd}}(r)$ is no longer prominent in $g^{FOD}(r)$ as may be expected by its reduced weighting. $g^{TMWD}(r)$ shows a clearly isolated peak at ≃ 1.8 Å that may be unambiguously associated with

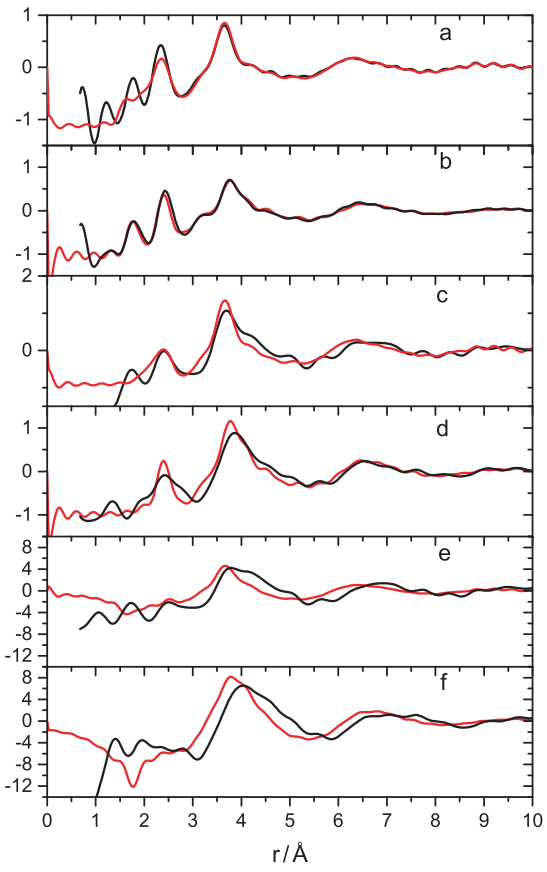

Figure 8: Comparison of the measured X-ray data (black) and the corresponding functions calculated from the MD-RMC data (red). a) $g^T(r)$ $Tb_3Al_5O_{12}$, b) $g^T(r)$ $Nd_3Al_5O_{12}$, c) $g^{FOD}(r)$ $Tb_3Al_5O_{12}$, d) $g^{FOD}(r)$ $Nd_3Al_5O_{12}$, e) $g^{TMWD}(r)$ $Tb_3Al_5O_{12}$ and f) $g^{TMWD}(r)$ $Nd_3Al_5O_{12}$.

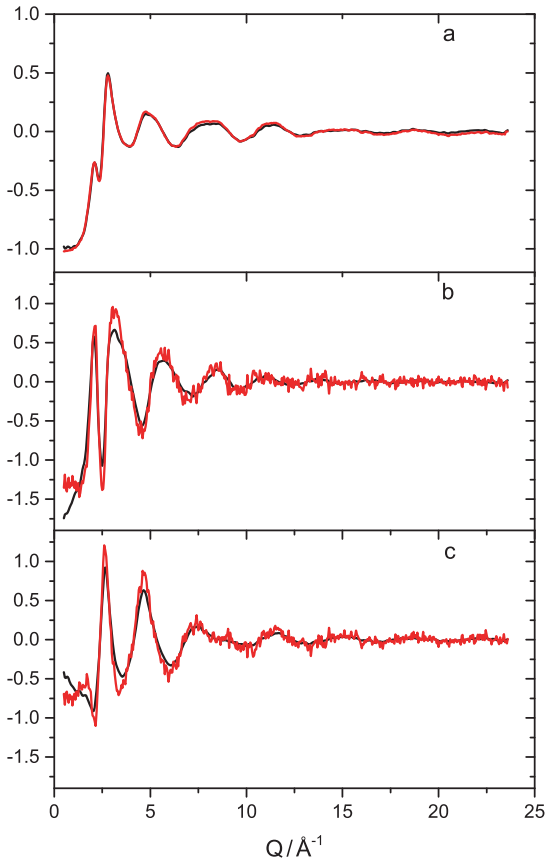

Figure 9: Comparison of the measured neutron data (black) and the corresponding functions calculated from the MD-RMC data (red) for $Nd_3Al_5O_{12}$. a) $S^T(Q)$, b) $S^{FOD}(Q)$ and c) $S^{TMWD}(Q)$.

$g_{\mathrm{AlO}}(r)$. Integration under this peaks gives a coordination number $n_{coord}^{\mathrm{AlO}} = 4.0(1)$. The peak at $\simeq 3$ Å may be associated principally with the first peak in $g_{OO}(r)$.

Figure 7 shows the X-ray diffraction patterns, $S^T(Q)$, $S^{FOD}(Q)$ and $S^{TMWD}(Q)$ measured for $Tb_3Al_5O_{12}$ and $Nd_3Al_5O_{12}$ compared with the final results of the MD-RMC refinement. It may been seen that good agreement has been achieved in $S^T(Q)$ and $S^{FOD}(Q)$ for both glasses. However, there are still some discrepancies

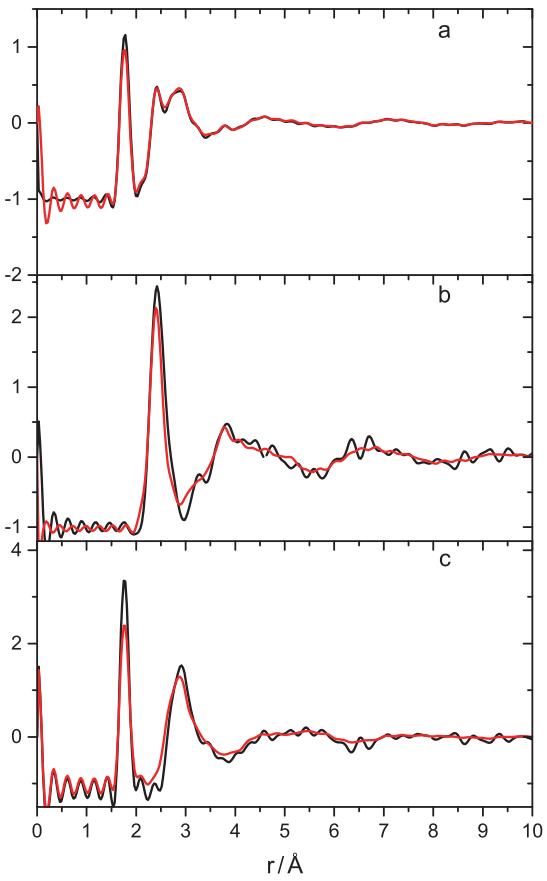

Figure 10: Comparison of the measured neutron data (black)and the corresponding functions calculated from the MD-RMC data (red) for $Nd_3Al_5O_{12}$. a) $g^T(r)$, b) $g^{FOD}(r)$ and c) $g^{TMWD}(r)$.

in $S^{TMWD}(Q)$, especially around the first peak. This is most likely due to the difficulty in achieving good normalization of the data and the remaining difficulties in treating the Q dependent form factors.

Figure 8 shows $g^T r$, $g^{FOD}(r)$ and $g^{TMWD}(r)$ for the data and the Fourier transform of the final MR-RMC refinements. It may be seen that the for $Nd_3Al_5O_{12}$ there is almost perfect agreement with the direct Fourier transform. However, in the case of $Tb_3Al_5O_{12}$ the result of the MD-RMC refinement is to give close agreement

with the first peak positions in $g_{TbO}(r)$ at $\simeq 2.3$ Å and $g_{TbTb}(r)$ at $\simeq 3.6$ Å. However, it also results in a significant broadening in the first peak in $g_{AlO}(r)$ that does not occur in the case of $Nd_3Al_5O_{12}$. At this point it should be remembered that in the case of $Tb_3Al_5O_{12}$ the original MD simulation was in much poorer agreement with the data and also that no neutron diffraction data was included in the refinement. The low weighting of the Al-Al, Al-O and O-O correlations in the X-ray data is most likely the origin of the this discrepancy and will be discussed later.

Figure 9 shows $S^T(Q)$, $S^{FOD}(Q)$ and $S^{TMWD}(Q)$ for the NDIS experiment and the final MD-RMC refinement for $Nd_3Al_5O_{12}$. It may be observed that the already good agreement between the experiment and the simulation has been improved slightly.

Figure 10 shows $g^T(r)$, $g^{FOD}(r)$ and $g^{TMWD}(r)$ for the Fourier transform of the experimental data and the result of the MD-RMC refinement for $Nd_3Al_5O_{12}$. The most notable change that has taken place in the real space data is the much better agreement of the third peak in $g^T(r)$ and the second peak in $g^{TMWD}(r)$.

5 Discussion

5.1 Direct methods

The amount of information that may be extracted from a *single* X-ray or neutron diffraction experiment by direct Fourier transform methods is limited to the case where resolved peaks may be identified, their peak positions calculated and by integration, the coordination number associated with the peak calculated. In this way, for example, it is possible to determine the Al-O coordination number in the $Nd_3Al_5O_{12}$ glass directly from the neutron $g^T(r)$ shown in Figure 6. However, determination of further peaks and coordination numbers is extremely limited by the numerous overlapping peaks above $\simeq 2.0$ Å. The Al-O peak may also be resolved in the X-ray $g^T(r)$ shown in Figure 4 although care must be taken to correct for the Q dependent form factors when calculating accurate coordination numbers. In addition, due to the high X-ray scattering factors for the rare-earth (RE) ion the nearest neighbour RE-O distance is also observed directly in the X-ray scattering data and the coordination number again calculated with careful normalization to correct form-factor weightings for this peak.

More detailed structural information may be obtained by additional diffraction experiments exploiting neutron diffraction and isotopic substitution (NDIS) or anomalous X-ray diffraction (AXD). The NDIS method has been long established and the extra information obtained can be seen in the clearly resolved Nd-

O peak in $g^{FOD}(r)$ and the Al-O peak in $g^{TMWD}(r)$ from which reliable distance and coordination number results were obtained.

In principle one may believe that similarly improved results should be obtained by AXD measurements. However, in the case of the glasses studied here the extra information obtained in the AXD measurements is more limited than the case of NDIS. It is true that the first order AXD difference formally eliminates the Al-Al, Al-O and O-O contributions to data but these are already very weak < 15% in the total diffraction data. Similarly the RE-RE correlation that dominates the total diffraction pattern dominates the first order difference function as well and the relative contributions of the RE-O and RE-Al correlations remain broadly similar. The TMWD function is also dominated by the RE-RE contributions and furthermore it is difficult to interpret due to the remaining complex Q dependence in the weighting factors (Figure 1). The reason for these observations is the high atomic number of the Rare-Earth (> 60) compared to Al(13) and O(8). Consideration of other systems suggests that AXD methods are best suited to systems where the atomic numbers of the elements are similar and in particular Se or Te glasses, as for example in the study of Fuoss et al. [6].

In contrast, in the NDIS experiment, where the neutron scattering lengths are broadly comparable, the First Order Difference method isolates the RE correlations (as in the case of AXD) and eliminates all Al-Al, Al-O and O-O correlations. Similarly, although there remains a RE-RE correlation in the TMWD, it is weak and $S^{TMWD}(Q)$ is dominated by the network Al-Al, Al-O and O-O correlations. Hence in the NDIS experiment, $S^{FOD}(Q)$ and $S^{TMWD}(Q)$ give complementary information related to the RE correlations to the network, and to the internal network correlations respectively.

A second isotope substitution has been used in the past to isolate the correlations of the target atom with itself; the so-called second order difference method [3]. In this context it may be noted in this particular case of Rare-Earth aluminate glasses, that the X-ray total diffraction experiment is dominated by this correlation. Furthermore its contrast may be enhanced by use of the AXD method such that X-ray measurements may be preferred over neutron diffraction if this correlation, in particular, is to be determined.

5.2 Modelling methods

As noted in the introduction, for an n component system, $n(n+1)/2$ distinct diffraction measurements are needed if the full set of $S_{\alpha\beta}(Q)$ for the system are to be determined. In practise this is not feasible due to the limited number of iso-

topes available and the numerical errors involved in solving the inverse matrix when $n > 2$.

An alternative approach to the direct methods discussed above is to use theoretical results to calculate expected diffraction patterns and to compare these with the experimental data. The most common methods are Monte-Carlo or Molecular Dynamics simulations that generate atomic configurations from which the $g_{\alpha\beta}(r)$ and hence $S_{\alpha\beta}(Q)$ may be calculated. These may be used to calculate the appropriate $S^T(Q)$, $S^{FOD}(Q)$ and $S^{TMWD}(Q)$ functions.

Figure 3 shows the comparison of MD simulations of $Tb_3Al_5O_{12}$ and $Nd_3Al_5O_{12}$ with the X-ray data with the potentials currently available. Although there is broad agreement, the comparison for $Nd_3Al_5O_{12}$ is clearly better than for $Tb_3Al_5O_{12}$. The origin of the difference for the Tb glass is seen clearly in Figure 4 where the second peak is shifted to lower r in the MD simulation. In contrast for $Nd_3Al_5O_{12}$ the agreement is very good apart from a small shoulder before the third peak in $g^T(r)$ that is not observed in the simulation data. The equally good agreement of the $Nd_3Al_5O_{12}$ simulation with the neutron diffraction data suggests, that in this case, the MD configuration is giving a good atomistic representation of the glass structure.

For the $Nd_3Al_5O_{12}$ data here the close agreement of the original MD simulation and the small changes in the atomic positions after the MD-RMC refinement give confidence that the final atomic configurations are a good representation of the glass structure. Hence it is possible to analyse the configuration to obtain, for example, coordination number distributions, bond angle distributions, partial structure factors, partial radial distribution functions and other structural information such as the network topology. Such analyses may be found in recent work on Barium Aluminate glasses[8], Barium Alumino-Titanate glasses [17] and liquid Alumina [10]. In this paper we do not discuss the final analysis of the $Tb_3Al_5O_{12}$ or $Nd_3Al_5O_{12}$ MD-RMC configurations but rather address the issue of the accuracy of the MD-RMC when there is a limited amount of diffraction data available.

In the analysis of the $Tb_3Al_5O_{12}$ data there was relatively poor agreement, in comparison to $Nd_3Al_5O_{12}$, of the MD simulation with the X-ray data obtained. Nevertheless, the MD configuration was refined successfully to obtain good agreement with experiment in both cases. In comparison however, the refinement of the $Tb_3Al_5O_{12}$ data resulted in relatively large movements of the atomic positions, so, given the weak Al-Al, Al-O and O-O contributions to the experimental data it raises the question about how well the final refined configuration reflects the structure of the glass in this case.

The more complete data set for the $Nd_3Al_5O_{12}$ glass allows us to address this question more directly. The close agreement with the MD simulation and the good

refinement, with small changes in the atomic positions, of the MD configuration when both the X-ray and neutron data are included gives us confidence that the refined configuration is a good representation of the glass structure. Hence we may use this configuration as a reference structure and compare it to results obtained for an analysis of the $Nd_3Al_5O_{12}$ glass when we use a more limited set of data for the MD-RMC refinement. More specifically, what happens if we only use the X-ray (including AXD) data for the MD-RMC refinement. This is equivalent to the $Tb_3Al_5O_{12}$ analysis we were able to carry out on the $Tb_3Al_5O_{12}$ glass.

When the $Nd_3Al_5O_{12}$ glass structure is refined by MD-RMC using X-ray data alone (including AXD) the fit is almost indistinguishable from that shown in Figure 7 and the quality of fit is similar to that obtained for $Tb_3Al_5O_{12}$. We used this MD-RMC configuration to generate predicted neutron diffraction patterns for our experimental data. These are shown in Figure 11. It is immediately noticeable that this refinement procedure results in a configuration that is in relatively poor agreement with the neutron data set and worse than our original MD simulation! Hence, in the example of these glasses it is clear that using X-ray data alone (even including AXD) is not sufficient to obtain a reliable atomic configuration via an MD-RMC refinement. The situation will be exacerbated in the case of $Tb_3Al_5O_{12}$ where the initial MD result was in much poorer agreement with the data. Hence, we do not believe the X-ray data for $Tb_3Al_5O_{12}$ collected here (even with AXD measurements) is sufficient to obtain a reliable atomistic configuration.

Figure 11 shows a comparison of the predicted NDIS results for $Nd_3Al_5O_{12}$ when a *single* neutron diffraction pattern is included in addition to the X-ray data. As expected the neutron $S^T(Q)$ is well refined but also the predicted neutron $S^{FOD}(Q)$ and $S^{TMWD}(Q)$ are now in good agreement with the measured data. Hence, in the case of $Tb_3Al_5O_{12}$ it can be concluded that the inclusion of a single total neutron diffraction measurement would enhance considerably the quality and reliability of the MD-RMC refinement, especially with regards to the accuracy of the network Al-Al, Al-O and O-O correlations. Clearly the addition of the NDIS measurement in this work enhances further the quality of the refinement.

The network structure may be explored further by considering the Bhatia-Thornton Structure factors for the Al-O network as described in previous studies [8, 17]. Figure 13 shows the results from the MD-RMC configurations of $Nd_3Al_5O_{12}$ and $Tb_3Al_5O_{12}$ compared with the results from the archetypal binary oxide glass GeO_2 [18]. $S_{CC}(Q)$ is broadly similar in all cases. $S_{NC}(Q)$ shows strong similarities for $Nd_3Al_5O_{12}$ and $Tb_3Al_5O_{12}$ but with more rapid damping at high Q compared to that observed in GeO_2. This confirms the network character in terms of Al-O bonds. However, there is a large difference observed in $S_{NN}(Q)$ for the $Nd_3Al_5O_{12}$ and $Tb_3Al_5O_{12}$ glasses. For the case of $Tb_3Al_5O_{12}$ the structure factor is more heavily damped at high Q and the strong peak observed at ~ 2.5 Å^{-1} in

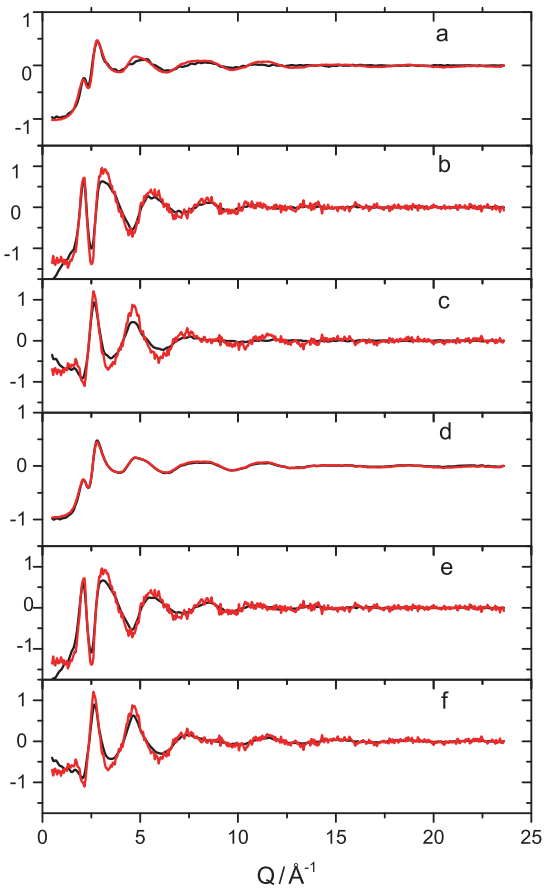

Figure 11: Comparison of the neutron diffraction measurements (black) to the predicted neutron patterns (red) for $Nd_3Al_5O_{12}$ when the the MD-RMC refinement was to the X-ray data alone a) $S^T(Q)$, b) $S^{FOD}(Q)$, c) $S^{TMWD}(Q)$ and when the data was refined with all the X-ray data and a single neutron diffraction measurement, d) $S^T(Q)$, e) $S^{FOD}(Q)$ and f) $S^{TMWD}(Q)$.

$Nd_3Al_5O_{12}$ is almost completely absent. $S_{NN}(Q)$ is strongly related to the network topology and given the similarity in their physical properties and their glass forming ability we would not expect such a large difference. As noted previously, the Al-O correlations are poorly weighted in the X-ray structure factors and this result

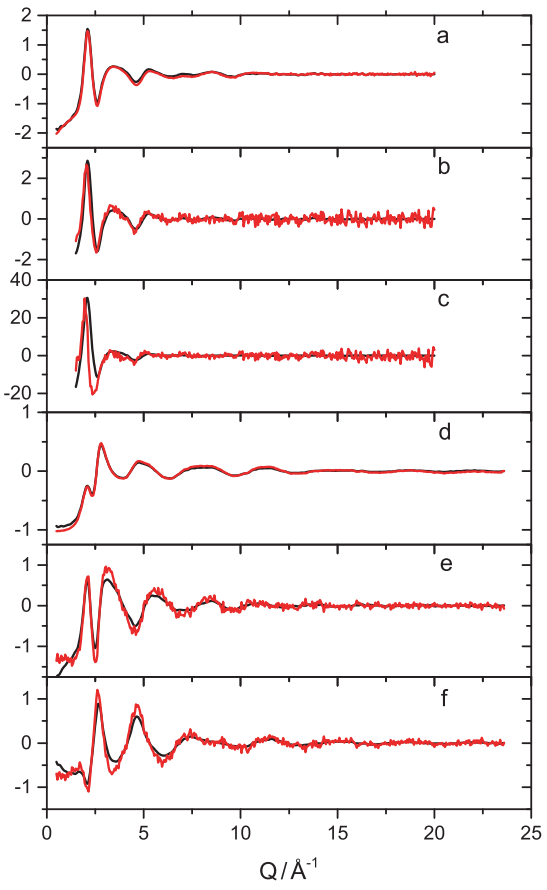

Figure 12: Comparison of the measured X-ray and neutron diffraction data (black) for $Nd_3Al_5O_{12}$ to the MD-RMC refinement (red) from a single X-ray and neutron diffraction pattern only. a) X-ray $S^T(Q)$, b) X-ray $S^{FOD}(Q)$, c) $S^{TMWD}(Q)$, d) neutron $S^T(Q)$, e) neutron $S^{FOD}(Q)$ and f) neutron $S^{TMWD}(Q)$.

confirms the observation above that the neutron data is essential, in this class of materials, to obtain meaningful information concerning the network structure.

It is interesting to compare $S_{NN}(Q)$ for $Nd_3Al_5O_{12}$ and that obtained for GeO_2. The structures are broadly similar except for the absence of a First Sharp Diffraction Peak (FSDP) at ~ 1.6 $Å^{-1}$ and the noticeably heavier damping of the

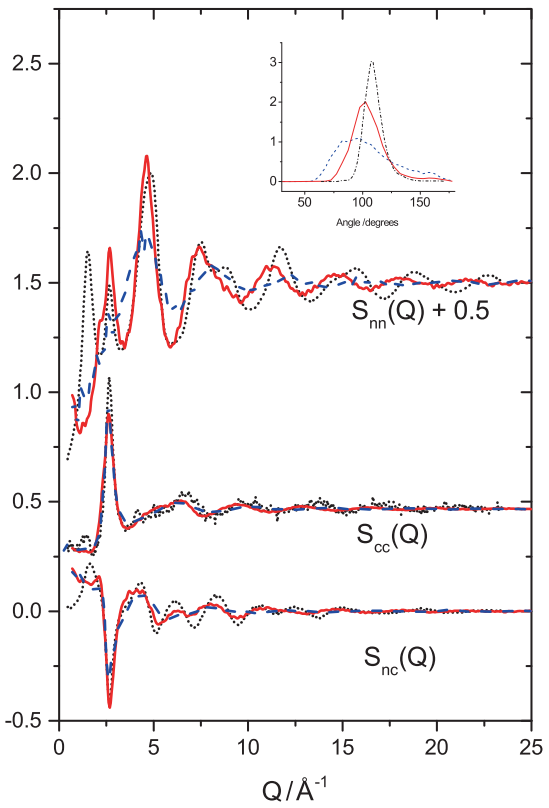

Figure 13: Comparison of the Bhatia–Thornton structure factors for GeO_2 (black dotted line), $Nd_3Al_5O_{12}$ (red (grey) solid line) and $Tb_3Al_5O_{12}$ (blue (black) dashed line) glass. The inset shows the O-Ge-O and O-Al-O bond angle distributions obtained from the MD-RMC configurations.

oscillations at high Q. This result is very similar to that observed in Ba-Al-Ti-O glasses [17] where higher coordinated Ti atoms and less uniform AlO_4 tetrahedra also resulted in the absence of a strong FSDP.

The Al-O coordination number obtained from the MD-RMC models using a cut-off of 2.1 Å gives a value of 4.0 and 4.1 for $Tb_3Al_5O_{12}$ and $Nd_3Al_5O_{12}$ respectively and confirms the basic 4-fold Al-O coordination. The inset in Figure 13 shows the O-Al-O bond angles compared to the O-Ge-O bond angle in GeO_2

glass. $Nd_3Al_5O_{12}$ shows a reasonably symmetric peak centred around 102° which is slightly smaller than the tetrahedral angle of 109°. This again suggests that the AlO_4 units are more distorted and not as rigid as observed in GeO_2 for which the angle corresponds to almost perfect tetrahedra. In comparison for $Tb_3Al_5O_{12}$ there is a broad distribution of angles that are more centred around 90° than 109°. This again confirms the difficulty of obtaining firm information concerning the Al-O coordination without the use of neutron scattering data.

Finally, it is interesting to compare the refinement result for the case in which only the total X-ray and neutron diffraction patterns are used for the MD-RMC refinement. This case is of particular interest as it avoids the need to carry out the technically challenging AXD measurements and the high cost of the isotopes necessary for the NDIS measurements. Figure 12 shows the refined Q-space data in this case. Comparison of this data with the MD-RMC refinement of the complete data set (Figures 7 and 9) shows good agreement, even in the difference functions that are not directly measured by this method.

This suggests that in the case of $Tb_3Al_5O_{12}$ a good quality atomistic configuration of the glass should be obtainable by making a complementary neutron diffraction measurement (isotopes do not exist in this case) and by obtaining an MD simulation that is closer agreement with the experimental data before the MD-RMC refinement is carried out.

5.3 Summary

The analysis of the $Nd_3Al_5O_{12}$ data above clearly demonstrates the need to include as much experimental data as possible in any MD-RMC refinement procedure. However, it must also be recognised there are limitations in the number of measurements that may be practically realised, for example, the lack of suitable isotopes for NDIS experiments.

Conventional analysis in terms of the interpretation of Fourier transformed $S(Q)$ data is limited in the case of Anomalous X-ray Diffraction data by the signal-to-noise ratio on the experimental data and the dominance of the RE-RE correlations in the total and the difference diffraction patterns. Nevertheless, for oxide glasses containing high atomic number metals this is a good method for measuring this correlation. In contrast NDIS provides high quality information on the nearest neighbour RE-O correlation in the First Order Difference and the Al-O nearest neighbour correlation in the Total Minus Weighted Difference measurement.

However, due to the Q-dependent form factors direct generation of X-ray/neutron difference functions is not possible. Hence, in order to make the max-

imum use of complementary X-ray and neutron diffraction data other methods must be explored.

The MD-RMC method is a suitable approach to combining neutron and X-ray data that avoids the problems associated with Q dependent X-ray form factors. The success of this method ultimately depends on the initial accuracy of the MD simulations and the information content in the experimental data. Comparative analysis of the $Nd_3Al_5O_{12}$ data in this paper shows the limits of relying on X-ray or neutron diffraction measurements alone (see for example Figure 11). Indeed, MD-RMC refinement in this case may give rise to a configuration that is in worse agreement than the original MD simulation.

For the case of the Rare-Earth glasses studied here, the most effective approach, when there is limited data available, is firstly to combine X-ray and neutron diffraction measurements at the total structure factor level. The results from the $Nd_3Al_5O_{12}$ measurements suggest that the MD-RMC refinement for $Tb_3Al_5O_{12}$ glass based on the X-ray diffraction measurements alone is insufficient to get a good atomistic model of the structure. However, it also suggests that for $Tb_3Al_5O_{12}$, where Tb isotopes do not exist, that the combination of X-ray and neutron total structure factor data, coupled with an improved MD simulation based on Morse potentials would be sufficient to generate a good atomistic model of this glass

If suitable Rare-Earth isotopes are available then a neutron first order difference measurement enhances strongly the available information due to the separation of the Rare-Earth correlations in the first order difference from the network contributions that dominate the Total Minus Weighted Difference function. However, restriction of the experimental data to NDIS alone (i.e. no X-ray data) means the RE-RE correlations are less constrained in the MD-RMC refinement. In principle, neutron second order difference methods can supply this information but this can only be done for a limited number of elements where suitable isotopes are available.

In comparison, MD-RMC refinement of X-ray diffraction measurements alone should be treated carefully even if AXD data is also included. In particular the low weighting of the Al-Al, Al-O and O-O means that little information about the glass network may be obtained from this method alone. Similarly, MD-RMC refinement of single neutron diffraction measurements is also prone to inaccuracies, especially with respect to the Rare-Earth correlations.

6 Conclusions

X-ray diffraction data including anomalous scattering measurements has been obtained for $Tb_3Al_5O_{12}$ glass. Neutron diffraction, including isotopic substitution (NDIS), and X-ray diffraction, including AXD, have been obtained for $Nd_3Al_5O_{12}$. Good agreement between and MD simulation based on Morse potentials and the $Nd_3Al_5O_{12}$ measurements was obtained. The MD configuration was further refined by the MD-RMC method to obtain a good atomistic description of the glass. It is shown, by comparable analysis of the $Nd_3Al_5O_{12}$ X-ray data alone that an MD-RMC refinement of the $Tb_3Al_5O_{12}$ data is incapable of refining the network structure of the glass, indeed it makes the situation worse. In general, the results demonstrate the need to consider carefully the information content (relative contributions of each correlation to the experimental data) when considering the ability of any MD-RMC refinement to accurately reflect the true structure of the material under study.

References

1. S. R. Elliot, *Physics of Amorphous Materials*, 2nd edn., Longman, Harlow, UK (1990).
2. M. Yamane and Y. Asahara, *Glasses for Photonics*, Cambridge University Press, Cambridge, UK (2000).
3. H. E. Fischer, A. C. Barnes, and P. S. Salmon, Rep. Prog. Phys. **69** (2006) 233.
4. A. C. Barnes, M. A. Hamilton, P. Buchanan, and M.-L. Saboungi, J. Non-Cryst. Solids **250–252** (1999) 393.
5. D. L. Price, M.-L. Saboungi, and A. C. Barnes, Phys. Rev. Lett. **81** (1998) 3207.
6. P. H. Fuoss, P. Eisenberger, W. K. Warburton, and A. Bienenstock, Phys. Rev. Lett. **46** (1981) 1537.
7. M. Hemmati, M. Wilson, and P. A. Madden, J. Phys. Chem. B **103** (1999) 4023.
8. L. B. Skinner, A. C. Barnes, P. S. Salmon, H. E. Fischer, J. W. E. Drewitt, and V. Honkimäki, Phys. Rev. B **85** (2012) 064201.
9. A. Zeidler, J. W. E. Drewitt, P. S. Salmon, A. C. Barnes, W. A. Crichton, S. Klotz, H. E. Fischer, C. J. Benmore, S. Ramos, and A. C. Hannon, J. Phys.-Condens. Mat. **21** (2009) 474217.
10. L. B. Skinner, A. C. Barnes, P. S. Salmon, L. Hennet, H. E. Fischer, C. J. Benmore, S. Kohara, J. K. R. Weber, A. Bytchkov, M. C. Wilding, J. B. Parise, T. O. Farmer, I. Pozdnyakova, S. K. Tumber, and K. Ohara, Phys. Rev. B **87** (2013) 024201.
11. A. C. Barnes, S. B. Lague, P. S. Salmon, and H. E. Fischer, J. Phys.-Condens. Mat. **9** (1997) 6157.
12. K. Wezka, A. Zeidler, P. S. Salmon, P. Kidkhunthod, A. C. Barnes, and H. E. Fischer, J. Non-Cryst. Solids **357** (2011) 2511.
13. W. Smith, and T. R. Forester, J. Mol. Graphics **14** (1996) 136.

14. W. Smith, T. R. Forester, I. T. Todorov, and M. Leslie, *The DL_POLY2 User Manual*, CCLRC Daresbury Laboratory, Daresbury, UK (2006).
15. T. S. Bush, J. D. Gale, C. R. A. Catlow, and P. D. Battle, J. Mater. Chem. **4** (1994) 831.
16. A. Pedone, G. Malavasi, M. C. Menziani, A. N. Cormack, and U. Segre, J. Phys. Chem. B **110** (2006) 11780.
17. P. Kidkhunthod, L. B. Skinner, A. C. Barnes, W. Klysubun, and H. E. Fischer, Phys. Rev. B **90** (2014) 094206.
18. P. S. Salmon, A. C. Barnes, R. A. Martin, and G. J. Cuello, J. Phys.-Condens. Mat. **19** (2007) 415110.
19. H. Rauch and W. Waschkowksi, *Neutron Data Booklet*, 2nd edn., chapt. 1.1, Old City Publishing, Philadelphia (2003).
20. E. N. Maslen, A. G. Fox, and M. A. O'Keefe, *International Tables for Crystallography*, chapt. 6.1.1, Kluwer Academic, Dordrecht (1995), p. 476.
21. M. G. Tucker, D. A. Keen, M. T. Dove, A. L. Goodwin, and Q. Hui, J. Phys.-Condens. Mat. **19** (2007) 335218.